

# DEL-Dock: Molecular Docking-Enabled Modeling of DNA-Encoded Libraries

Kirill Shmilovich,<sup>†,¶</sup> Benson Chen,<sup>‡,¶</sup> Theofanis Karaletsos,<sup>\*,‡</sup> and Mohammad  
M. Sultan<sup>\*,‡</sup>

<sup>†</sup>*Pritzker School of Molecular Engineering, University of Chicago, Chicago, Illinois 60637,  
United States*

<sup>‡</sup>*Insitro, South San Francisco, California 94080, United States*

<sup>¶</sup>*Equal Contribution*

E-mail: theofanis@insitro.com; msultan@insitro.com

## Abstract

DNA-Encoded Library (DEL) technology has enabled significant advances in hit identification by enabling efficient testing of combinatorially-generated molecular libraries. DEL screens measure protein binding affinity through sequencing reads of molecules tagged with unique DNA-barcodes that survive a series of selection experiments. Computational models have been deployed to learn the latent binding affinities that are correlated to the sequenced count data; however, this correlation is often obfuscated by various sources of noise introduced in its complicated data-generation process. In order to denoise DEL count data and screen for molecules with good binding affinity, computational models require the correct assumptions in their modeling structure to capture the correct signals underlying the data. Recent advances in DEL models have focused on probabilistic formulations of count data, but existing approaches have thus far been limited to only utilizing 2-D molecule-level representations. We introduce a new paradigm, DEL-Dock, that combines ligand-based descriptors with 3-D spatial information from docked protein-ligand complexes. 3-D spatial information allows our model to learn over the actual binding modality rather than using only structure-based information of the ligand. We show that our model is capable of effectively denoising DEL count data to predict molecule enrichment scores that are better correlated with experimental binding affinity measurements compared to prior works. Moreover, by learning over a collection of docked poses we demonstrate that our model, trained only on DEL data, implicitly learns to perform good docking pose selection without requiring external supervision from expensive-to-source protein crystal structures.

# Introduction

One key component of early drug discovery is hit identification, or finding molecules with desired activity levels and properties of interest.<sup>1</sup> This task has been commonly approached via high-throughput screening (HTS) techniques, which involve testing a library of molecules against a biological target of interest. While traditional screening techniques do not scale well to large chemical spaces, DNA-encoded library (DEL) technologies provide one avenue towards the desired scale. For instance, while traditional HTS libraries typically contain only  $\sim 50\text{k}$ - $5\text{M}$  compounds, DELs enable screening of combinatorially large molecular spaces that allow for testing  $\sim 1\text{M}$ - $5\text{B}$  compounds in a single tube.<sup>2,3</sup> By capturing a broad chemical diversity landscape, DEL technology has opened new opportunities in hit identification.<sup>4-7</sup>

DELs are constructed by sequentially assembling molecular building blocks, aka synthons, into molecules tagged with unique DNA-barcode identifiers (Fig. 1). Once synthesized, the library is tested for affinity against a protein of interest through a series of selection experiments. This process, called panning, typically involves spiking the DEL into a solution of the immobilized protein, and washing the resulting mixture for multiple rounds. This procedure leaves members of the library that remain bound to either the target or matrix, which are subsequently identified using next-generation DNA sequencing. The resulting data after bioinformatics processing consists of sparse reads of the DNA and the corresponding molecules; the relative abundance of the identified molecules is, in theory, a reasonable proxy for their binding affinities. However, DEL data from panning experiments contain various sources of noise such as matrix binding, truncation products, unequal initial loads, replicate and sequencing biases.<sup>8-11</sup> Modeling the data without considering these significant sources of noise can overfit to spurious correlations. Consequently, while DELs have proven to be powerful tools in drug discovery, careful consideration of the appropriate techniques to denoise DEL data is required to discover reliable signals of the underlying small molecule binding affinities.

Several approaches have been developed to tackle DEL modeling from a computational

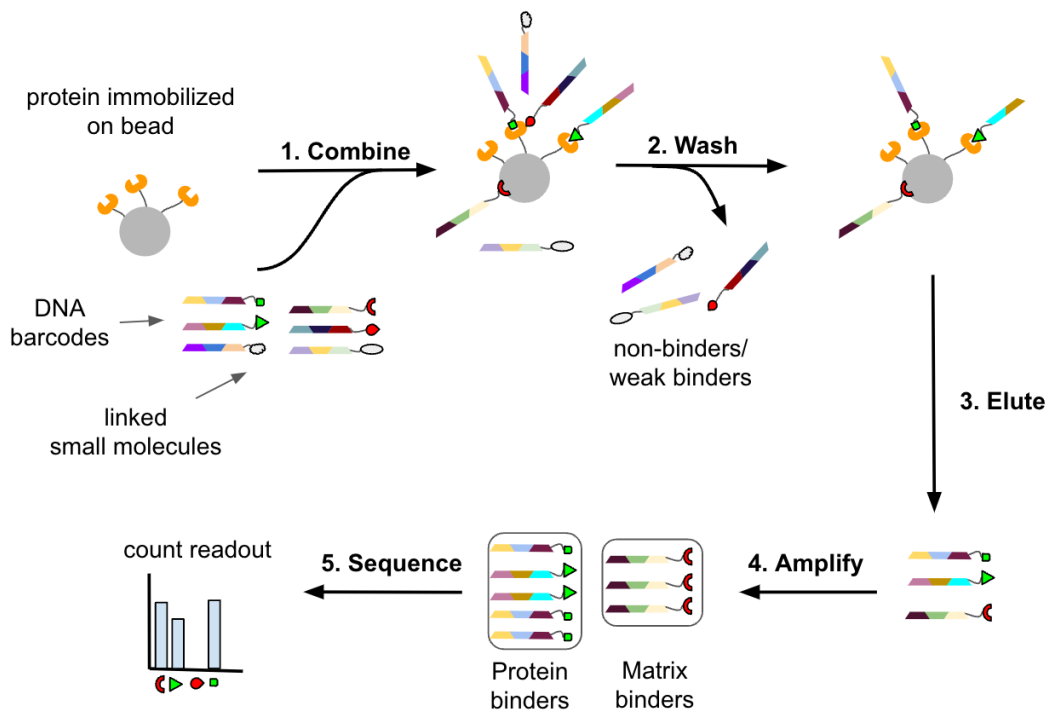


Figure 1: Step-by-step diagram of a DNA-Encoded Library (DEL) panning experiment.

perspective: these existing methods rely on computing an **enrichment score** for each molecule that is representative of its binding affinity to the protein target. One approach for calculating enrichment scores involves fitting a Poisson distribution to observed on-target and control count data for each molecule and then formulating enrichment scores as ratios of these Poisson parameters.<sup>12</sup> A deficiency in this enrichment metric is that it neglects to include any structural information of the actual DEL molecules. Since molecular structure represents an important aspect for determining protein-ligand interactions,<sup>13,14</sup> other methods incorporate different types of molecular representations into their models. McCloskey et al.<sup>15</sup> use a Graph Neural Network (GNN) to encode molecules, formulating the learning problem as multi-class binary classification over the counts. Recent methods consider hybrid approaches that combine molecular representation learning with probabilistic modeling.<sup>8,9,16</sup> Central to these approaches involves modelling observed sequencing counts as originating from latent Poisson or Gamma-Poisson distributions, which are well suited to describe independently distributed count events. This allows the models to incorporate the inherent noise

in the data-generating process within the model structure. However, these methods focus on learning only representations of the molecules themselves and omit the rich representation of the 3-D protein-ligand interactions which are critical aspects for describing protein binding.

In order to leverage 3-D spatial data, we turn to molecular docking, which has a long history of being an important tool in structure-based drug discovery.<sup>17</sup> A key component of these docking methods is to define a scoring function that can characterize the binding interactions between a protein and ligand. To generate candidate poses, these methods use the aforementioned scoring function to sample ligand conformations with the goal of ultimately inferring the most likely binding mode. While there have been many advances to docking models and software, in practice, there are still many pitfalls of these methods.<sup>18</sup> For instance, the difficulty of the docking problem can be observed through the low empirical correlation between high scoring docked poses and actual binding affinity.<sup>19</sup> Improvements can be realized through carefully calibrated scoring functions, but tuning these scoring functions is frequently problem-specific and involves substantial domain knowledge.<sup>20-22</sup> ML-enabled scoring functions trained on databases of crystal structures have recently demonstrated improved performance in some settings,<sup>23</sup> however, these approaches are ultimately limited by scarce and expensive-to-generate crystal structures. Even though docking generates noisy ligand conformations, these docking techniques can provide a useful distribution of likely binding poses which we will exploit in our new ideas for modeling DEL count data.

Towards the goal of more holistic DEL models, we propose DEL-Dock, a model that directly learns a joint protein-ligand representation by synthesizing multi-modal information within a unified probabilistic framework to learn enrichment scores. Our approach combines molecule-level descriptors with spatial information from docked protein-ligand complexes to explain sequencing counts. We delineate contributions from spurious matrix binding and target protein binding to better separate the signal from noise in the data. Additionally, our model can learn to rank a collection of poses without explicit supervision of pose scores by only training on the count data. When viewed separately, DEL data and docked poses

provide noisy signals of binding affinity, but our DEL-Dock model effectively combines these two modalities to better extract the learning signals from the data.

In this work, we engage the commonly studied protein human carbonic anhydrase (CAIX) by training our model on publicly available DEL data generated by Gerry et al.<sup>12</sup>. On a held-out evaluation data set of 3041 molecules with experimental affinity measurements extracted from the BindingDB<sup>24</sup> web database, we demonstrate our approach effectively learns enrichment scores that are well correlated with binding affinity. Moreover, we show that our model is capable of extracting insights into the determinants of docked protein-ligand complexes that are most influential for protein binding.

## Methods

Our model combines two different representation modalities, molecule-level descriptors and docked protein-ligand complexes, to capture the latent aspects of protein binding from a probabilistic perspective (Fig. 2). The combinatorial construction of DELs motivates using expressive molecular representations to capture statistical correlation between the building block substructures used in DEL synthesis. We use Morgan fingerprint, calculated with RDKit (version 2020.09.1),<sup>25</sup> as basis for our molecular representations, which is a standard descriptor for representational problems on small molecules<sup>26</sup> and also provide the added benefit of their simple construction and rapid processing. Morgan fingerprints compute a structural bit hash of the molecule by enumerating  $k$ -hop substructures about each atom. Since there are many shared structural features across different molecular compounds, these fingerprints constitute a simple representation that has demonstrated remarkable empirical performance throughout cheminformatic domains. We represent docked protein-ligand poses using a pretrained voxel-based CNN model from GNINA, which captures spatial relationships by discretizing space into three-dimensional voxels and leveraging CNNs to learn complex hierarchical representations.<sup>27-29</sup> The CNN models used in this work was originally trained

on the PDBBind<sup>30</sup> database, capitalizing on this supervised data source to capture the important features that characterize protein-ligand interactions.

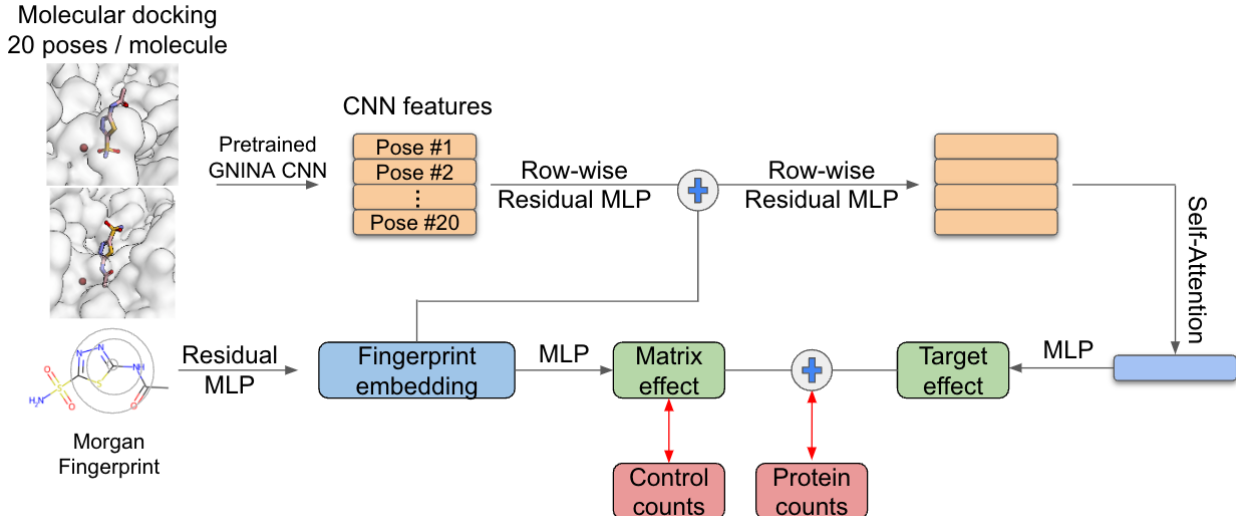


Figure 2: Schematic illustration of our DEL-Dock neural network architecture and data flow.

Let  $\mathcal{X}$  denote the set of molecules in our data, where each molecule  $x \in \mathcal{X}$  has an associated set of  $n$  docked poses  $\{p_1, p_2, \dots, p_n\} \in \mathcal{P}$  and  $c_i^{\text{matrix}} \in C^{\text{matrix}}, c_i^{\text{target}} \in C^{\text{target}}$  are the  $i$ th replicates (repeated experiments) of count data from the beads-only control and target protein experiments respectively. Additionally, we can define the following featurization transformations that are used to construct the molecule and pose embeddings:  $\Phi : \mathcal{X} \rightarrow [0, 1]^{n_\phi}$  is the function that generates a  $n_\phi$ -bit molecular fingerprint; here, we use a 2048-bit Morgan fingerprint with radius 3.  $\Psi : \mathcal{X} \times \mathcal{P} \rightarrow \mathbb{R}^{n_\psi}$  is the transformation that outputs an embedding of the molecule and a specific spatial protein-ligand complex, where we use a pre-trained voxel-based CNN to perform this transformation.

Let  $h^{\text{fps}} = \text{MLP}(\Phi(x))$  be the molecule embedding learned by our model, which is computed by applying a multilayer perceptron (MLP) to the fingerprint representation. Individual docked pose embeddings are similarly computed, with one difference being that we also incorporate the fingerprint embedding,  $h_i^{\text{pose}} = \text{MLP}([\Psi(x, p_i); h^{\text{fps}}])$  into this representation.

To synthesize the set of poses for each molecule we apply a self-attention layer over the

pose embeddings. Following previous work on self-attention and multiple-instance learning (MIL),<sup>31</sup> we compute attention weights in eq. (1), where  $(w, W^U, W^V)$  are learnable weights,  $\sigma$  is the sigmoid activation and  $\odot$  is element-wise multiplication. The final output pose embedding that combines information from the individual input poses is then computed as a attention-score weighted embedding vector  $h^{\text{pose}} = \frac{1}{n} \sum_i a_i h_i^{\text{pose}}$ .

$$a_i = \frac{\exp \left[ w \cdot (\tanh(W^U h_i^{\text{pose}}) \odot \sigma(W^V h_i^{\text{pose}})) \right]}{\sum_j \exp \left[ w \cdot (\tanh(W^U h_j^{\text{pose}}) \odot \sigma(W^V h_j^{\text{pose}})) \right]} \quad (1)$$

Equipped with these molecule and pose embeddings, our model learns the contributions of both spurious matrix binding and target protein binding by predicting latent scores that strive to maximize the likelihood of the observed data under the model. We make several distinct modeling choices to mirror our assumptions about the data-generation process that accounts for various sources of experimental noise.

**Matrix Binding** is a confounding factor inherent to DEL experiments, since molecules are prone to binding to the multifarious components comprising the immobilized matrix in addition to the intended protein target. For each molecule  $x$ , we learn a latent matrix binding score  $\lambda^{\text{matrix}} = f(h^{\text{fps}})$ . Since matrix binding is not a function of the protein-ligand pose representation, we enforce that the matrix binding enrichment remains only a function of the molecule embedding  $h^{\text{fps}}$ .

**Target Binding** is learned through  $\lambda^{\text{target}} = f(h^{\text{pose}})$ , jointly utilizing both molecule and pose representations. This design choice reflects that sequencing counts from the target protein experiment must be a function of both small molecule binding to the protein receptor, represented here as featurizations of the docked protein-ligand complexes, along with promiscuous binding to the immobilized matrix.

The observed count data for both the control and protein target experiments can be modeled as originating from underlying Poisson distributions, which naturally characterize any discrete count data from independently sampled events. Due to possible sequencing

noise we further augment this basic Poisson model as a zero-inflated probability distribution. This design choice is motivated by the chance that sparse zero counts in the data could be explained as an artifact of imperfect sequencing technology, and as a result we directly incorporate this assumption into the structure of our model. We note that previous approaches have employed Gamma-Poisson distributions to model DEL count data in the past,<sup>16</sup> but we make the assumption here that replicate data for the same molecule is sampled from an identical distribution.

$$P(C = c|\lambda, \pi) = \begin{cases} \pi + (1 - \pi)e^{-\lambda} & \text{if } c = 0 \\ (1 - \pi)\frac{\lambda^c e^{-\lambda}}{c!} & \text{if } c > 0 \end{cases} \quad (2)$$

$$C^{\text{matrix}} \sim \text{ZIP}(\lambda^{\text{matrix}}, \pi^{\text{matrix}}) \quad \lambda^{\text{matrix}} = \exp(\text{MLP}(h^{\text{fps}})) \quad (3)$$

$$C^{\text{target}} \sim \text{ZIP}(\lambda^{\text{matrix}} + \lambda^{\text{target}}, \pi^{\text{target}}) \quad \lambda^{\text{target}} = \exp(\text{MLP}(h^{\text{pose}})) \quad (4)$$

Let  $C$  be distributed as a zero-inflated Poisson (ZIP), with its probability density function (PDF) defined in eq. (2). Here,  $\lambda$  is the rate parameter of the underlying Poisson distribution, and  $\pi$  denotes the occurrence of choosing the zero distribution, and is taken to be the empirical average (when  $\pi = 0$ , this reduces to the typical Poisson distribution). Empirically, we estimate these zero-count probabilities from the zero-count frequencies in the control ( $\pi^{\text{matrix}} \approx 0.0075$ ) and protein target ( $\pi^{\text{target}} \approx 0.55$ ) experiments. Since we model the control and protein experiments as originating from separate underlying count distributions, we compute two distinct rate parameters for each ZIP distribution as shown in eq. (3). The observed target counts is a function of both matrix binding and binding to the protein target, so the rate parameter for the target distribution is a function of  $\lambda^{\text{matrix}}$  and  $\lambda^{\text{target}}$ . We assume an additive functional form for the latent matrix and target enrichments, which we find works well empirically. We note however that there could be more motivated methods

to parameterize the interactions of matrix and target binding. The final loss function is then a typical negative log-likelihood (NLL) loss over the observed counts from both the control and target experiments eq. (5).

$$L = - \sum_i \log [P(c_i^{\text{matrix}} | \lambda^{\text{matrix}}, \pi^{\text{matrix}})] - \sum_j \log [P(c_j^{\text{target}} | \lambda^{\text{target}} + \lambda^{\text{matrix}}, \pi^{\text{target}})] \quad (5)$$

## DEL Data

To train our model we use publicly available DEL data collected by Gerry et al.<sup>12</sup>. This tri-synthon library consists of  $\sim 100\text{k}$  molecules with count data for panning experiments for the human carbonic anhydrase IX (CAIX) protein. In addition to on-target counts, the data includes beads-only no-target controls. Four replicate sets of counts for the protein target experiments are provided, while two replicates of the control experiments are provided in this data set. To account for possible noise in different replicates, we follow previous work and normalize the counts for each target and control replicate by dividing each count by the sum of counts in that replicate experiment and then multiplying by  $1\text{e}6$  to re-calibrate the scale of the counts.<sup>16</sup> This data preprocessing provides the interpretation of each molecule count as a molecular frequency of that molecule within the DEL library. The processed data set is then used to train our models employing a 80/10/10 - train/validation/test split. Complete training details are further provided in the Supporting Information.

## Evaluation Data

We evaluate the performance of our models on benchmarks using an external set of affinity measurements of small molecule curated from the BindingDB<sup>24</sup> web database. We queried binding affinities for the Human Carbonic anhydrase 9 (CAIX) protein target (UniProt: Q16790), and kept only molecules containing the same atom types as those present in the DEL data set (C, O, N, S, H, I). This external evaluation data set is composed of 3041 small

molecules with molecular weights ranging from  $\sim 25$  amu to  $\sim 1000$  amu and associated experimental inhibitory constant ( $K_i$ ) measurements ranging from  $\sim 0.15$  M to  $\sim 90$  pM. We use the median affinity value in the cases where multiple different affinity measurements were reported for the same molecule. We also consider a subset of this dataset which consists of the 521 molecules with molecular weights between 417 amu and 517 amu (Fig. 6 in the Supporting Information). These molecular weights correspond to the interquartile range bounding the 10th and 90th percentiles of the molecular weights in training dataset. This restricted subset presents a more challenging test as differentiation cannot rely on only extensive properties such as molecular weight, but must also effectively identify chemical motifs that impact molecular binding within this tightly bound range of molecular weights. We notice that simple properties such as molecular weight or benzenesulfonamide presence, which is known to be an important binding motif for carbonic anhydrase,<sup>12,32,33</sup> achieve better baseline performance on the full evaluation data compared to the restricted subset. These metrics suggest that this subset is more challenging as predictors must learn beyond these simple molecular properties to achieve good performance.

## Docking

We perform molecular docking to generate a collection of ligand-bound poses to a target protein of interest for all molecules within in our training and evaluation data sets. Docking is performed using the GNINA docking software<sup>27-29</sup> employing the Vina<sup>34</sup> scoring function. All molecules are docked against CAIX (PDB:5FL4) with the location of the binding pocket determined by the bound crystal structure ligand (9FK), using the default GNINA settings defining an  $8 \times 8 \times 8 \text{ \AA}^3$  bounding box around this ligand. Initial three-dimensional conformers for all docked molecules were generated with RDKit. For each molecule, we obtain 20 docked poses from GNINA using an exhaustiveness parameter of 50, using the Vina scoring for end-to-end pose generation. This approach can similarly be performed using AutoDock Vina<sup>34</sup> or Smina<sup>35</sup> using the Vina scoring function.

# Results

We demonstrate that our model outperforms previous systems on DEL enrichment prediction by jointly combining topological features from the molecular graph and the spatial 3-D protein-ligand information, and additionally illustrate the capability of our model to better rank ligand poses compared to traditional docking. Our model learns latent binding affinity for each molecule to both the matrix and the target as the denoised signals compared to the observed count data. In this interpretation we should expect higher enrichment scores predicted by our model to be well-correlated with binding affinity, and therefore provide a useful metric for predicting anticipated protein binding in virtual screening campaigns.

## **DEL-Dock outperforms baselines using only docking or molecule-level descriptors**

To evaluate the performance of our model, especially with respect to out-of-domain protein binding prediction, we first train our model on DEL data screened against the human carbonic anhydrase IX (CAIX) protein target,<sup>12</sup> and then predict enrichment scores for molecules with externally measured experimental binding affinities to CAIX. We evaluate performance in this setting by measuring spearman rank-correlation coefficients between predicted enrichments and the experimental affinity measurements, which is a metric that is agnostic to the scale of the values. Our model only restricts the enrichment scores to be positive quantities, with no specific distributional constraints, so spearman rank-correlation, which computes a correlation based only on the ordinal ranking of the predicted enrichments, is well suited for our test scenario.

Our method, DEL-Dock, which combines information from docked complexes with molecular descriptors outperforms previous techniques which only utilize one of these two data modalities (see Table 1). We find that traditional docking scores alone generated from AutoDock Vina<sup>34</sup> result in the worst overall correlations, commensurate with previous ob-

servations that docking scores alone are typically not reliable predictors of binding affinity.<sup>19</sup> Performance based on docked poses alone is however greatly improved when re-scoring the docked poses using pretrained GNINA<sup>36</sup> CNN models. Another set of baselines we consider are DEL models that rely only on molecular descriptors. First, we consider a simple model that involves training a random forest (RF) on the Morgan fingerprints using the enrichment metrics originally formulated to facilitate analysis of the DEL data set by Gerry et al.<sup>12</sup>.

We then similarly predict the enrichment scores of molecules in the held-out dataset and the correlation with experimental Ki data. This baseline achieves reasonable performance on both the full and subset evaluation data, especially given the simplicity of the model. For a more sophisticated baseline, we train the Graph Neural Network (GNN) model with the DEL-specific loss function defined by Lim et al.<sup>9</sup> While this approach achieves good performance on the full evaluation data, correlations on the restricted subset are largely unchanged for all docking-based and molecular descriptor-based baselines. Our model which combines docking pose embeddings with molecular fingerprint representations outperforms all other baselines, with the largest improvements of  $\sim 2\times$  better spearman correlations than other approaches realized on the more challenging molecular weight restricted subset. We provide further ablation studies of our model in the Supporting Information.

## **DEL-Dock better ranks molecules with known binding chemical motifs**

While our approach displays good prediction accuracy with respect to experimental binding measurements, we also find our model provides insights into the structural and chemical factors that influence binding. Compounds containing benzenesulfonamide have been well established in literature as the primarily chemical motif that drives small molecule binding to carbonic anhydrase.<sup>12,32,33</sup> Though we do not explicitly incorporate this as a learning signal for our model, we observe that our model is able to learn this association, visibly predicting sulfonamides within our evaluation data set as more highly enriched compared

Table 1: Comparison of spearman rank-correlation coefficients between predicted affinity scores and experimental inhibition constant ( $K_i$ ) measurements curated from BindingDB.<sup>24</sup> Spearman correlations are shown for the complete 3041-molecule data set (full), and a 521-molecule subset of this full data set confined to molecular weights between 417-517 amu. This molecular weight range approximately corresponds to the 10<sup>th</sup> and 90<sup>th</sup> interquartile range of the molecular weights spanned by the DEL data set. Error bars are reported as standard deviations over five independently initialized models.

Model	Spearman Ki (full) ↓	Spearman Ki (subset) ↓
Molecular weight	-0.121	0.074
Benzenesulfonamide presence	-0.199	-0.063
Top Vina <sup>34</sup> docking score	-0.068	0.119
Top GNINA <sup>36</sup> docking score	-0.279 ± 0.044	-0.091 ± 0.061
RF trained on enrichment scores from ( Gerry et al. <sup>12</sup> )	-0.231 ± 0.007	-0.091 ± 0.012
GNN ( Lim et al. <sup>9</sup> )	-0.298 ± 0.005	-0.075 ± 0.011
<b>DEL-Dock (ours)</b>	<b>-0.328 ± 0.01</b>	<b>-0.186 ± 0.01</b>

molecules which do not contain benzenesulfonamides (Fig. 3a). Interestingly, we observe a comparatively large fraction of non-benzenesulfonamides identified as good binders with low experimental  $K_i$ . The elevated population of highly enriched non-benzenesulfonamides in this data set could be an artifact of bias in scientific literature. Our model is ultimately trained on DEL data and therefore is expected to reflect underlying biases and idiosyncrasies of the data generation process. The most notable difference lies in that DEL experiments are only capable of measuring on-DNA binding, while the evaluation data are measurements of off-DNA binding. Nevertheless, the clear delineation of benzenesulfonamides in our predicted enrichments provides good *post-hoc* evidence that our model correctly identifies this important binding motif for this protein target.

An important structural component of benzenesulfonamides binding to carbonic anhydrase is coordination of the sulfonamide group with the zinc ion buried within the active site.<sup>12,32,33</sup> In the vast majority of cases, one would then expect docking scoring functions to highly score poses that reflect this anticipated binding mode. As our model performs self-attention over pose embeddings, which are used to learn molecules’ enrichment scores, we can interpret the magnitude of the attention probabilities as the importance weight of that

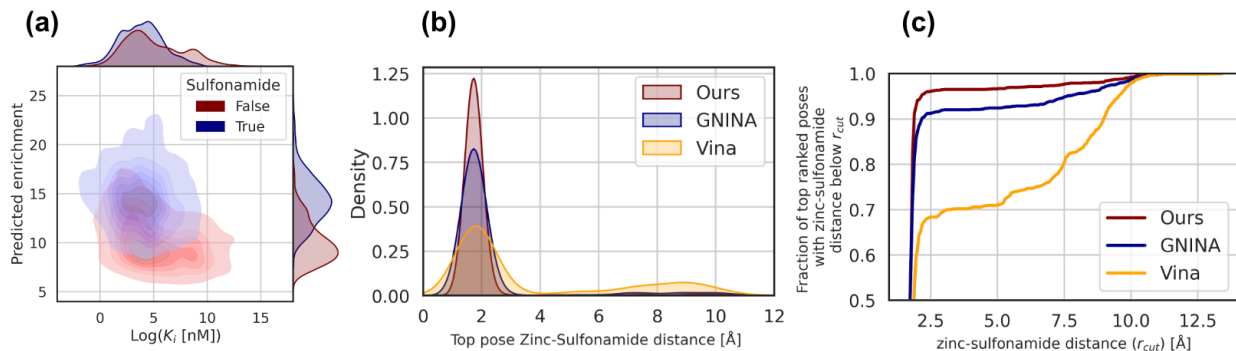


Figure 3: Analysis of DEL-Dock model predictions on our evaluation data set composed of experimental affinity ( $K_i$ ) measurements. **(a)** Parity plot of our model predicted enrichments and ground truth  $K_i$  measurements delineated by benzenesulfonamide presence, with 1581 benzenesulfonamide-containing molecules and 1460 non-benzenesulfonamide. **(b)** Distribution of zinc-sulfonamide distances for the top-ranked pose of each benzenesulfonamide in our evaluation data set identified by the AutoDock Vina scoring function,<sup>34</sup> GNINA pose selection,<sup>36</sup> and our model predicted attention scores. **(c)** Comparison in the fraction of top ranked poses identified with with zinc-sulfonamide distance below a threshold distance between  $\sim 2$ - $12\text{\AA}$ . This can be interpreted as the CDF of the distributions in **(b)** with the appropriate normalization.

particular pose. Shown in Fig. 3b is the distribution of zinc-sulfonamide distances for the top-selected docked pose comparing AutoDock Vina, GNINA, and our method for all 1581 benzenesulfonamides-containing molecules in our evaluation data set. An alternate view of this data is presented as the fraction of top-selected poses with zinc-sulfonamide distances below a distance threshold (Fig. 3c), which can effectively be interpreted as the cumulative distribution function (CDF) of the appropriately normalized associated probability distribution function (PDF) in Fig. 3b.

The AutoDock Vina scoring function exhibits largest spread of zinc-sulfonamide distances, and as a result identifying a comparatively large fraction of poses as incorrectly coordinated. GNINA pose selection performs significantly better in this setting, identifying a larger fraction of well-coordinated poses with low zinc-sulfonamide distance. We find our method ultimately correctly coordinates the largest proportion of poses when compared to AutoDock Vina or GNINA. We note that our approach for binding pose selection is markedly different than the approach taken by GNINA, which involves a separate pose scoring head

trained to identify poses with low-RMSD to ground truth crystal structures. Our attention scores on the other hand are effectively latent variables trained only via the auxiliary task of modeling DEL data. The benefit of our approach is that we can learn to identify good poses in an unsupervised manner, without requiring scarce and expensive crystal structures to serve as the source of supervision for pose selection.

## **DEL-Dock offers interpretability through its attention mechanisms**

Lastly, we further demonstrate the interpretability of our model by examining the distribution of attention scores learned by our model for a specific molecule (Fig. 4). For this molecule, only 7 out of 20 docked poses correctly coordinate the sulfonamide group with the zinc ion buried in the protein active site. Our model appropriately identifies this binding mode and learns attention scores that more favorably rank these 7 correctly coordinated poses (Fig. 4). The top-three ranked poses (Fig. 4a) by our model have very similar conformations, each exhibiting zinc-sulfonamide coordination, and differing only in the orientation of the terminal benzene ring that is distant from the active site. The other poses that show zinc-sulfonamide coordination (Fig. 4b-d) are also ranked highly by our model, however, these poses exhibit less favorable conformations in several ways. For instance, the conformation in Fig. 4b is more exposed, and less protected by the protein. Finally, our model in general more poorly ranks poses that display incorrect zinc-sulfonamide coordination (Fig. 4e). These conformations typically have the terminal benzene ring inserted into the active site. Also, these poses reveal why zinc-sulfonamide distances alone can be a deceiving metric as some poses are capable of achieving low zinc-sulfonamide distances ( $\sim 3$  Å) due to the molecule “curling in” on itself within the active site. Nevertheless, our model recognizes this spurious binding mode and poorly ranks these poses with comparatively low attention scores, even though AutoDock Vina highly ranks many of these bad poses. Overall, we find the hierarchy of pose rankings by our model to be commensurate with anticipated binding behavior for this protein target.

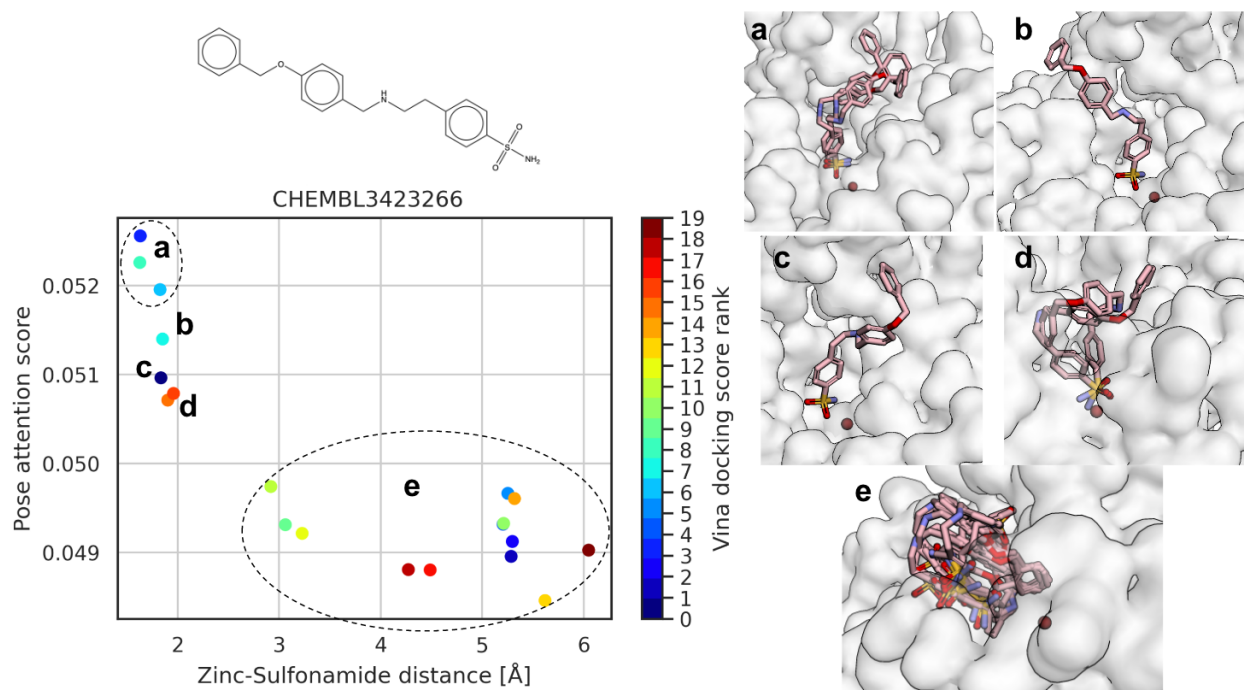


Figure 4: Analysis of pose attention scores for a representative molecule in our evaluation data set. (left) Our model predicted pose attention scores plotted against the zinc-sulfonamide distance of the docked pose and colored according to the ranking determined by the AutoDock Vina scoring function. (right) Different protein-ligand complexes are visualized to show that our model highly ranks the conformers with zinc-sulfonamide coordination (a-d), while the conformers without the correct coordination are ranked lower (e).

## Conclusions

In this work we present an approach for modeling DEL data that combines docking-based and molecular descriptor-based data modalities. Our approach involves predicting two interleaved quantities, enrichment scores, that explain the sequencing counts of the panning experiment measurements for both the on-target protein and the off-target control beads. We evaluate our method by first training on DEL data screened against the human carbonic anhydrase (CAIX)<sup>12</sup> protein target, and then predicting binding for unseen molecules with external experimental constant of inhibition ( $K_i$ ) affinity measurements curated from the BindingDB<sup>24</sup> web database. For this prediction task we find our approach outperforms previous docking and DEL modeling techniques that only use either docked poses or molecular descriptor information alone. Furthermore, a critical component of our model involves performing self-attention over pose embedding, in order to learn over the set of possible poses. Analyzing these latent attention scores, we find our model effectively identifies good docked poses. Compared to docking pose selection using either AutoDock Vina<sup>34</sup> or GNINA,<sup>27-29,36</sup> our model more reliably selects poses displaying the appropriate zinc-sulfonamide coordination—which is known to be the predominant binding mode for carbonic anhydrase.<sup>12,32,33</sup> Our model is interestingly capable of learning good pose selection in an unsupervised manner, training only on the voluminous DEL data rather than requiring crystal structures to serve as the source of supervision.

There are some limitations to our approach, however. Our approach assumes that we can obtain reasonably accurate protein-ligand docking poses, which is not always true. We can only utilize this model for proteins which have 3-D crystal structures; and even if protein crystal structures are available, they may not always be accurate. Additionally, we are limited by the quality of the docking software, which may fail to capture the actual correct binding modes, or ranking the good binding modes highly.

Our work focuses on introducing the concept of utilizing docked poses to improve DEL models, but there are several avenues for future work. While we use Morgan fingerprints

as our molecule featurizer, deep learning approaches have the potential to generate more expressive representations, such as Graph Neural Networks (GNNs) that have demonstrated excellent predictive performance on many molecular property prediction tasks.<sup>37</sup> In our application, equivariant GNNs could also be used as an alternative featurizer to CNNs for embedding docked poses, which would provide the added benefit of producing explicitly roto-translationally symmetric representations.<sup>38</sup> We only select the top ranking poses from docking, but providing a more diverse set of poses could be more useful instead. Future research directions could also leverage our approach to unsupervised pose selection for downstream free energy calculations in larger-scale virtual screening campaigns. Our approach paves the way for multi-modality modeling of DEL data and unsupervised learning of bespoke, DEL-conditioned, scoring functions.

## Acknowledgements

We would like to thank Nathaniel Stanley and Sam Mun at Insitro for helpful discussions and advice related to Docking software and usage. We would also like to thank Daphne Koller, Robert Hilgraf, Nathaniel Stanley, Fiorella Ruggiu and Yujia Bao at Insitro for providing general feedback and review of our work. Lastly, we would like to thank Patrick Conrad at Insitro for helping us with the public code release.

## Data Availability

We use publicly available data from Gerry et al.<sup>12</sup>, and our code is publicly available at: <https://github.com/insitro/insitro-research>.

# Supporting Information

## Training settings

Featurizations for the docked poses are generated using pre-trained GNINA models provided in `gnina-torch`.<sup>28,29</sup> The `dense` variant of the GNINA models composed of densely connected 3D residual CNN blocks introduced in Francoeur et al.<sup>36</sup> are used to generate 224-dimensional embeddings of each docked pose. Morgan fingerprints<sup>26</sup> for each molecule are calculated using `RDKit` with a radius of 3 embedded into a 2048 dimensional bit-vector.

All models are trained end-to-end using mini-batch gradient descent with the Adam optimizer<sup>39</sup> and coefficients for the running averages of  $\beta_1 = 0.95$  and  $\beta_2 = 0.999$ . A batch size of 64 is used with an initial learning rate of  $1 \times 10^{-4}$  and a linearly decaying learning rate scheduler where the learning rate is decayed by a factor of  $\gamma^{\frac{1}{n_{steps}}}$  every batch. For our learning rate scheduler we use  $\gamma = 0.1$  and  $n_{steps} = 1250$ , which corresponds to a  $10\times$  reduction in the learning rate after 1250 batches. We also apply gradient clipping, where gradient norms are clipped to a maximum value of 0.1. During training we maintain an exponential moving average over our model parameters which are updated each step with a decay rate of 0.999. This exponential moving average version of the model parameters is then used for evaluation and throughout all inference tasks. Throughout our model we use LeakyReLU activation functions with a negative slope constant of  $1 \times 10^{-2}$ , except for the final activation function applied to the output logits corresponding to the matrix and target enrichment scores where we apply an exponential function as our terminal activation. A hidden dimensionality of 256 is used within MLP layers in our network. The residual MLP layers, which are responsible for processing the Morgan fingerprints along with the CNN features and embeddings (Fig. 2 in the main text), are composed of 2 residually connected MLP layers using dropout with a probability of 0.5. Our model in sum is composed of  $\sim 1\text{M}$  parameters and is trained for 8 epochs on a single NVIDIA T4 GPU. A PyTorch implementation of our model that makes use of PyTorch Lightning<sup>40</sup> and Pyro<sup>41</sup> is publicly available

at: <https://github.com/insitro/insitro-research>.

## Ablations

We present here a number of ablations on our model, exploring some different architectural components and design choices (Table 2). First, we see that training models with only fingerprint representations, without incorporating any information from the docked poses, results in a marked decrease in performance. On the other hand models, trained using only CNN representations perform much better and display comparable performance to only GNINA pre-trained models (Table 1). This represents an intuitive result, as this training setting is effectively equivalent to fine-tuning GNINA using a multi-instance learning over the pose representations. Interestingly, we find that training on the CNN features alone already achieves good binding pose selection based on the latent attention scores, a feature our model is evidently capable of learning in isolation of the fingerprint representations. Also shown as a baseline is the MLP network trained using the bespoke loss function for modelling DEL data presented by Lim et al.<sup>9</sup>. This approach represents the lower performing of the two architectures explored by Lim et al.<sup>9</sup>, the other being the GNN architecture presented as a baseline in the main text (Table 1).

Table 2: Model ablations and other baselines. Error bars are calculated as standard deviations over five independently initialized models.

Model	Spearman Ki (full) ↓	Spearman Ki (subset) ↓
Only fingerprints	$-0.191 \pm 0.005$	$-0.083 \pm 0.019$
Only CNN	$-0.287 \pm 0.005$	$-0.124 \pm 0.006$
MLP from Lim et al. <sup>9</sup>	$-0.244 \pm 0.004$	$-0.076 \pm 0.017$
Without zero-inflated distribution	$-0.26 \pm 0.02$	$-0.08 \pm 0.03$
End-to-end voxels with frozen CNN	$-0.278 \pm 0.022$	$-0.16 \pm 0.03$

Interestingly using a zero-inflated loss appears to be critical to our performance, resulting in  $\sim 25\%$  increase in spearman rank-correlation on the full evaluation set and greater than

a  $2\times$  increase on the subset. We suspect this performance jump could be related to the disparity in zero-counts between the control and on-target experiment: the control experiments have a zero-count frequency of  $\sim 0.75\%$  while the protein target experiments have a zero-count frequency of  $\sim 55\%$ . Using a zero-inflated distribution could provide our model more flexibility to explain zero-counts as an artifact of the data generation process, rather than an outcome of poor protein binding.

Instead of using pre-computed CNN features from GNINA we also explored training our model directly from the voxel representations using frozen CNN featurizers. The benefit of this approach is the ability to use data augmentation via random rotations and translations to implicitly enforce that the learned CNN embeddings remain roto-translationally equivariant. While we notice performance on the evaluation subset is comparable with our trained on pre-computed CNN features (Table 1), the performance on the full data set is slightly reduced. We suspect this result could be due to the computational challenges of using voxelized representations. In particular, when training over many docked poses (in our case 20 poses per molecule) our batch size is effectively  $20\times$  larger – which presents a significant memory bottleneck as the voxel representation requires storing a  $48\times 48\times 48\times 28$  molecular grids (three dimensions discretizing space, and one for different atom types). Furthermore, our pre-computed features are already being generated with pre-trained CNN featurizers that have been trained using data augmentation, albeit on PDBBind for the separate task of affinity and pose prediction. Nevertheless, we certainly expect improved performances could still be achieved for these full differentiable training approaches given the appropriate compute resources and further tuning.

Lastly, presented in Table 3 is a comparison of spearman rank-correlation performances training on variable numbers of poses. For each model the top- $k$  poses generated via docking are used for training. Performance tends to generally improve with increasing number of poses used for training, with the largest difference in improvements realized on the molecular weight restricted subset. Beyond  $\sim 10$  poses appears to result in diminishing returns, in

comparison to the jumpy in improvements seen from 2  $\rightarrow$  10 poses.

Table 3: Model ablations training on different numbers of docked poses. Error bars are calculated as standard deviations over five independently initialized models.

Number of training poses	Spearman Ki (full) $\downarrow$	Spearman Ki (subset) $\downarrow$
2 poses	$-0.278 \pm 0.011$	$-0.112 \pm 0.023$
5 poses	$-0.304 \pm 0.01$	$-0.15 \pm 0.02$
10 poses	$-0.318 \pm 0.007$	$-0.175 \pm 0.02$
15 poses	$-0.324 \pm 0.008$	$-0.182 \pm 0.014$
20 poses	$-0.328 \pm 0.009$	$-0.186 \pm 0.013$

## Supplementary Figures

Shown in Fig. 5 is a TSNE embedding of the DEL data set alongside our evaluation data. This TSNE embedding is generated by representing each molecule with a concatenation of three fingerprint representations: a 2048-dimensional Morgan fingerprint with a radius of 3, 167-dimensional MACCS (Molecular ACCess System) fingerprint, and finally a 2048-dimensional atom pair fingerprint. All fingerprints are calculated using `RDKit`. `Sci-kit learn` is then used to generate the TSNE embedding using a `tanimoto` similarity metric with a perplexity of 30 trained on the combined DEL and evaluation data. We notice the evaluation data is largely isolated from the DEL data in this TSNE embedding, serving as an indication that our evaluation data is markedly different, or out of domain, than the DEL data used in training our models.

Shown in Fig. 7 are the distributions of zinc-sulfonamide distances throughout the top-five ranking poses as identified by our DEL-DOCK model attention scores, GNINA pose selection, and the AutoDock Vina scoring function. We notice that the highly ranked poses by our model attribute more density in the closely separated regime under  $\sim 4\text{\AA}$  than GNINA or Vina, and as a direct consequence of this we see fewer poses selected by our model showing large separations between  $\sim 4\text{\AA}$  -  $\sim 13\text{\AA}$ .

### TSNE Embedding of DEL and evaluation data

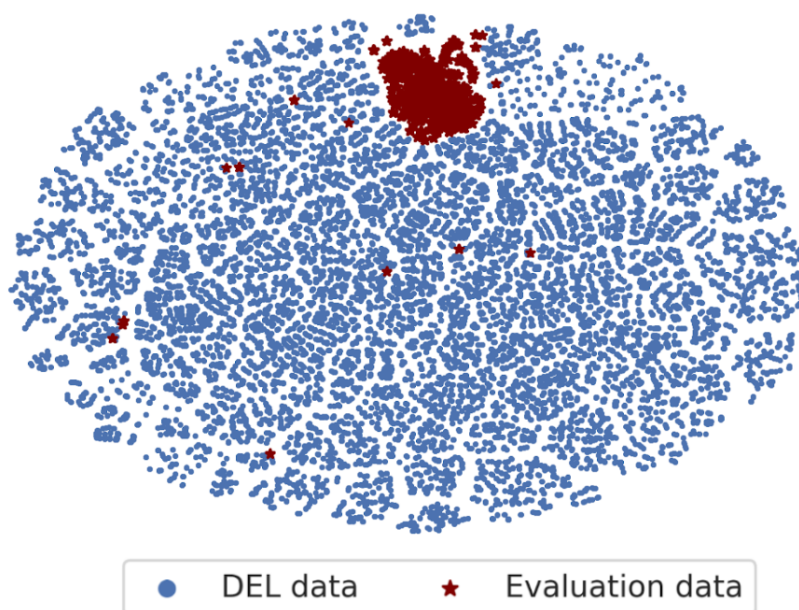


Figure 5: TSNE embedding our of DEL and evaluation data. Molecular representations for this TSNE embedding are generated as a concatenation of three fingerprint representations: Morgan fingerprints, MACCS fingerprints, and atom pair fingerprints.

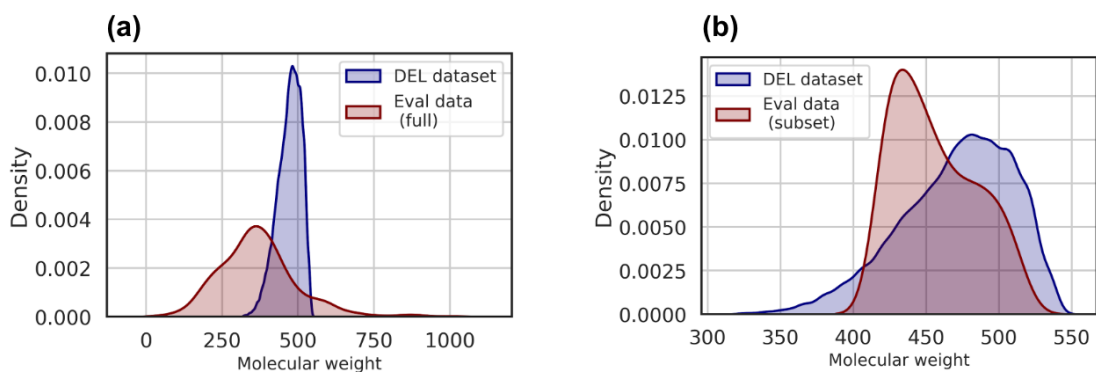


Figure 6: Comparison of the distribution of molecular weights between the DEL data set and (a) the full evaluation data set and (b) the 417-517 amu subset of the evaluation data set. Distributions are generated as a Kernel Density Estimate (KDE) plot as implemented in `seaborn`.<sup>42</sup>

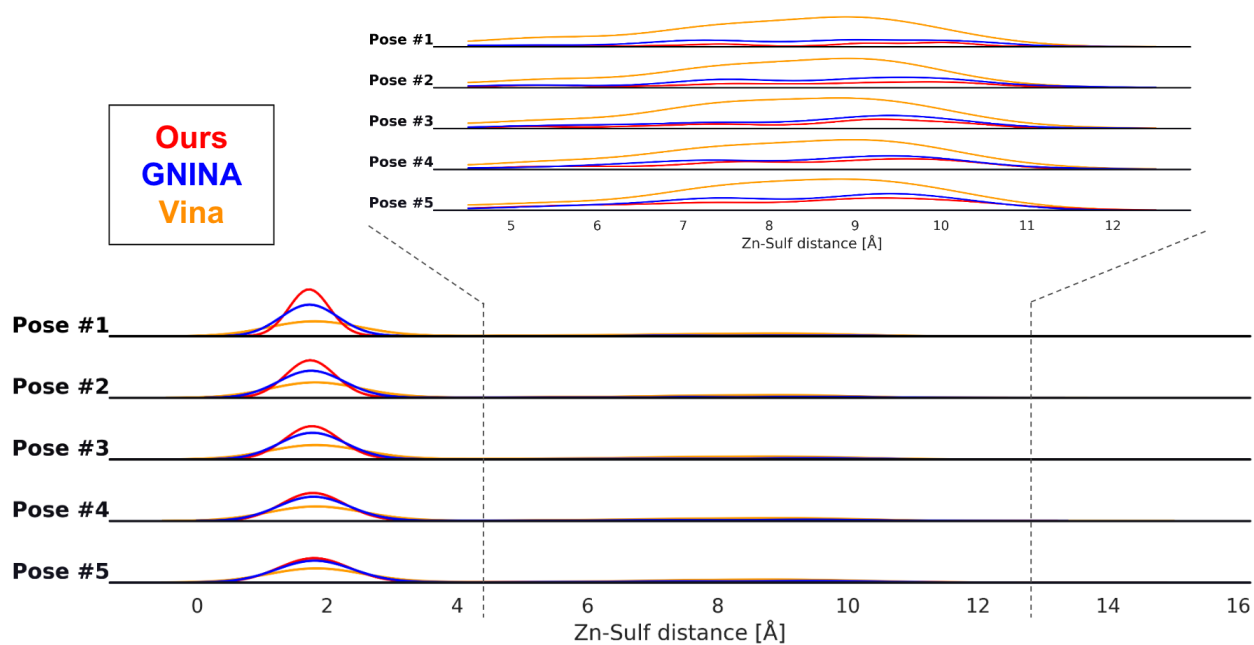


Figure 7: Distribution of Zinc-Sulfonamide distances throughout the top-five ranked poses by our DEL-DOCK model attention scores, GNINA pose selection score, and AutoDock Vina scoring function.

## References

- (1) Hughes, J. P.; Rees, S.; Kalindjian, S. B.; Philpott, K. L. Principles of early drug discovery. *British journal of pharmacology* **2011**, *162*, 1239–1249.
- (2) Satz, A. L.; Brunschweiler, A.; Flanagan, M. E.; Gloger, A.; Hansen, N. J.; Kuai, L.; Kunig, V. B.; Lu, X.; Madsen, D.; Marcaurelle, L. A., et al. DNA-encoded chemical libraries. *Nature Reviews Methods Primers* **2022**, *2*, 1–17.
- (3) Sunkari, Y. K.; Siripuram, V. K.; Nguyen, T.-L.; Flajolet, M. High-power screening (HPS) empowered by DNA-encoded libraries. *Trends in Pharmacological Sciences* **2021**,
- (4) Clark, M. A.; Acharya, R. A.; Arico-Muendel, C. C.; Belyanskaya, S. L.; Benjamin, D. R.; Carlson, N. R.; Centrella, P. A.; Chiu, C. H.; Creaser, S. P.; Cuzzo, J. W.,

- et al. Design, synthesis and selection of DNA-encoded small-molecule libraries. *Nature chemical biology* **2009**, *5*, 647–654.
- (5) Kleiner, R. E.; Dumelin, C. E.; Liu, D. R. Small-molecule discovery from DNA-encoded chemical libraries. *Chemical Society Reviews* **2011**, *40*, 5707–5717.
- (6) Goodnow, R. A.; Dumelin, C. E.; Keefe, A. D. DNA-encoded chemistry: enabling the deeper sampling of chemical space. *Nature Reviews Drug Discovery* **2017**, *16*, 131–147.
- (7) Flood, D. T.; Kingston, C.; Vantourout, J. C.; Dawson, P. E.; Baran, P. S. DNA encoded libraries: a visitor’s guide. *Israel Journal of Chemistry* **2020**, *60*, 268–280.
- (8) Binder, P.; Lawler, M.; Grady, L.; Carlson, N.; Leelananda, S.; Belyanskaya, S.; Franklin, J.; Tilmans, N.; Palacci, H. Partial Product Aware Machine Learning on DNA-Encoded Libraries. *arXiv preprint arXiv:2205.08020* **2022**,
- (9) Lim, K. S.; Reidenbach, A. G.; Hua, B. K.; Mason, J. W.; Gerry, C. J.; Clemons, P. A.; Coley, C. W. Machine learning on DNA-encoded library count data using an uncertainty-aware probabilistic loss function. *Journal of Chemical Information and Modeling* **2022**,
- (10) Zhu, H.; Foley, T. L.; Montgomery, J. I.; Stanton, R. V. Understanding Data Noise and Uncertainty through Analysis of Replicate Samples in DNA-Encoded Library Selection. *Journal of Chemical Information and Modeling* **2021**, *62*, 2239–2247.
- (11) Kómár, P.; Kalinic, M. Denoising DNA encoded library screens with sparse learning. *ACS Combinatorial Science* **2020**, *22*, 410–421.
- (12) Gerry, C. J.; Wawer, M. J.; Clemons, P. A.; Schreiber, S. L. DNA barcoding a complete matrix of stereoisomeric small molecules. *Journal of the American Chemical Society* **2019**, *141*, 10225–10235.

- (13) Jones, D.; Kim, H.; Zhang, X.; Zemla, A.; Stevenson, G.; Bennett, W. D.; Kirshner, D.; Wong, S. E.; Lightstone, F. C.; Allen, J. E. Improved protein–ligand binding affinity prediction with structure-based deep fusion inference. *Journal of chemical information and modeling* **2021**, *61*, 1583–1592.
- (14) Hwang, H.; Dey, F.; Petrey, D.; Honig, B. Structure-based prediction of ligand–protein interactions on a genome-wide scale. *Proceedings of the National Academy of Sciences* **2017**, *114*, 13685–13690.
- (15) McCloskey, K.; Sigel, E. A.; Kearnes, S.; Xue, L.; Tian, X.; Moccia, D.; Gikunju, D.; Bazzaz, S.; Chan, B.; Clark, M. A., et al. Machine learning on DNA-encoded libraries: a new paradigm for hit finding. *Journal of Medicinal Chemistry* **2020**, *63*, 8857–8866.
- (16) Ma, R.; Dreiman, G. H.; Ruggiu, F.; Riesselman, A. J.; Liu, B.; James, K.; Sultan, M.; Koller, D. Regression modeling on DNA encoded libraries. NeurIPS 2021 AI for Science Workshop. 2021.
- (17) Meng, X.-Y.; Zhang, H.-X.; Mezei, M.; Cui, M. Molecular docking: a powerful approach for structure-based drug discovery. *Current computer-aided drug design* **2011**, *7*, 146–157.
- (18) Chen, Y.-C. Beware of docking! *Trends in pharmacological sciences* **2015**, *36*, 78–95.
- (19) Gupta, M.; Sharma, R.; Kumar, A. Docking techniques in pharmacology: How much promising? *Computational biology and chemistry* **2018**, *76*, 210–217.
- (20) Li, J.; Fu, A.; Zhang, L. An overview of scoring functions used for protein–ligand interactions in molecular docking. *Interdisciplinary Sciences: Computational Life Sciences* **2019**, *11*, 320–328.
- (21) Pham, T. A.; Jain, A. N. Customizing scoring functions for docking. *Journal of Computer-Aided Molecular Design* **2008**, *22*, 269–286.

- (22) Jain, A. N. Scoring noncovalent protein-ligand interactions: a continuous differentiable function tuned to compute binding affinities. *Journal of computer-aided molecular design* **1996**, *10*, 427–440.
- (23) Wallach, I.; Dzamba, M.; Heifets, A. AtomNet: a deep convolutional neural network for bioactivity prediction in structure-based drug discovery. *arXiv preprint arXiv:1510.02855* **2015**,
- (24) Liu, T.; Lin, Y.; Wen, X.; Jorissen, R. N.; Gilson, M. K. BindingDB: a web-accessible database of experimentally determined protein–ligand binding affinities. *Nucleic acids research* **2007**, *35*, D198–D201.
- (25) Landrum, G. et al. rdkit/rdkit: 2020\_09\_1 (Q3 2020) Release. 2020; <https://doi.org/10.5281/zenodo.4107869>.
- (26) Rogers, D.; Hahn, M. Extended-connectivity fingerprints. *Journal of chemical information and modeling* **2010**, *50*, 742–754.
- (27) McNutt, A. T.; Francoeur, P.; Aggarwal, R.; Masuda, T.; Meli, R.; Ragoza, M.; Sunseri, J.; Koes, D. R. GNINA 1.0: molecular docking with deep learning. *Journal of cheminformatics* **2021**, *13*, 1–20.
- (28) Ragoza, M.; Hochuli, J.; Idrobo, E.; Sunseri, J.; Koes, D. R. Protein–ligand scoring with convolutional neural networks. *Journal of chemical information and modeling* **2017**, *57*, 942–957.
- (29) Sunseri, J.; Koes, D. R. Libmolgrid: graphics processing unit accelerated molecular gridding for deep learning applications. *Journal of chemical information and modeling* **2020**, *60*, 1079–1084.
- (30) Liu, Z.; Su, M.; Han, L.; Liu, J.; Yang, Q.; Li, Y.; Wang, R. Forging the basis for

- developing protein–ligand interaction scoring functions. *Accounts of chemical research* **2017**, *50*, 302–309.
- (31) Ilse, M.; Tomczak, J.; Welling, M. Attention-based deep multiple instance learning. International conference on machine learning. 2018; pp 2127–2136.
- (32) Li, Y.; De Luca, R.; Cazzamalli, S.; Pretto, F.; Bajic, D.; Scheuermann, J.; Neri, D. Versatile protein recognition by the encoded display of multiple chemical elements on a constant macrocyclic scaffold. *Nature chemistry* **2018**, *10*, 441–448.
- (33) Buller, F.; Steiner, M.; Frey, K.; Mirsof, D.; Scheuermann, J.; Kalisch, M.; Bühlmann, P.; Supuran, C. T.; Neri, D. Selection of carbonic anhydrase IX inhibitors from one million DNA-encoded compounds. *ACS chemical biology* **2011**, *6*, 336–344.
- (34) Trott, O.; Olson, A. J. AutoDock Vina: improving the speed and accuracy of docking with a new scoring function, efficient optimization, and multithreading. *Journal of computational chemistry* **2010**, *31*, 455–461.
- (35) Koes, D. R.; Baumgartner, M. P.; Camacho, C. J. Lessons learned in empirical scoring with smina from the CSAR 2011 benchmarking exercise. *Journal of chemical information and modeling* **2013**, *53*, 1893–1904.
- (36) Francoeur, P. G.; Masuda, T.; Sunseri, J.; Jia, A.; Iovanisci, R. B.; Snyder, I.; Koes, D. R. Three-dimensional convolutional neural networks and a cross-docked data set for structure-based drug design. *Journal of chemical information and modeling* **2020**, *60*, 4200–4215.
- (37) Stokes, J. M.; Yang, K.; Swanson, K.; Jin, W.; Cubillos-Ruiz, A.; Donghia, N. M.; MacNair, C. R.; French, S.; Carfrae, L. A.; Bloom-Ackermann, Z., et al. A deep learning approach to antibiotic discovery. *Cell* **2020**, *180*, 688–702.

- (38) Stärk, H.; Ganea, O.; Pattanaik, L.; Barzilay, R.; Jaakkola, T. Equibind: Geometric deep learning for drug binding structure prediction. *International Conference on Machine Learning*. 2022; pp 20503–20521.
- (39) Kingma, D. P.; Ba, J. Adam: A method for stochastic optimization. *arXiv preprint arXiv:1412.6980* **2014**,
- (40) Falcon, W. et al. PyTorchLightning/pytorch-lightning: 0.7.6 release. 2020; <https://doi.org/10.5281/zenodo.3828935>.
- (41) Bingham, E.; Chen, J. P.; Jankowiak, M.; Obermeyer, F.; Pradhan, N.; Karaletsos, T.; Singh, R.; Szerlip, P.; Horsfall, P.; Goodman, N. D. Pyro: Deep universal probabilistic programming. *The Journal of Machine Learning Research* **2019**, *20*, 973–978.
- (42) Waskom, M. L. seaborn: statistical data visualization. *Journal of Open Source Software* **2021**, *6*, 3021.